

Perfect one-dimensional chiral states in biased twisted bilayer graphene

Bonnie Tsim,^{1,2} Nguyen N. T. Nam,³ and Mikito Koshino⁴

¹*National Graphene Institute, University of Manchester, Manchester M13 9PL, UK*

²*Department of Physics and Astronomy, University of Manchester, Manchester M13 9PL, UK*

³*Mathematics for Advanced Materials Open Innovation Lab (MathAM-OIL), AIST, Sendai 980-8577, Japan*

⁴*Department of Physics, Osaka University, Toyonaka 560-0043, Japan*

We theoretically study the electronic structure of small-angle twisted bilayer graphene with a large potential asymmetry between the top and bottom layers. We show that the emergent helical states known to appear on the triangular AB-BA domain boundary do not actually form a percolating network, but instead they provide independent, perfect one-dimensional channels propagating in three different directions. Using the continuum-model Hamiltonian, we demonstrate that an applied bias causes two well-defined energy windows which contain sparsely distributed one-dimensional channels. The origin of these energy windows can be understood using a two-band model of the intersecting electron and hole bands of single layer graphene. We also use the tight-binding model to implement the lattice deformations in twisted bilayer graphene, and discuss the effect of lattice relaxation on the one-dimensional channels.

I. INTRODUCTION

Twisted bilayer graphene (TBG) consists of two layers of graphene overlaid on top of each other with a relative twist between their crystallographic axes. A moiré interference pattern which emerges from the overlap of the two mismatched graphene lattices results in a strong modification of the electronic structure by the superlattice band folding^{1–10}. The system has been shown to exhibit many interesting physical phenomena and, since the realisation of superconductivity and correlated insulating states in magic-angle TBG^{11–13}, there has been a huge surge of theoretical and experimental research in this field.

In this paper, we theoretically study the electronic structure of small-angle TBG with a large interlayer bias (i.e., potential asymmetry between the top and bottom layers), and demonstrate the formation of perfect one-dimensional (1D) states within well-defined energy windows on either side of zero energy. The effect of the interlayer bias on TBG was investigated in the previous works^{14–18}, and it was found that a large enough bias gives rise to a helical network of chiral channels on the domain boundaries between AB and BA stacking regions¹⁵. There the electronic states at AB and BA regions are locally gapped out by the interlayer bias¹⁹, and two helical modes per spin and per valley necessarily appear on each AB-BA boundary^{20,21}, reflecting that the two regions have different quantized values of single-valley Hall conductivity, $\pm e^2/h$.²² In TBG, the AB and BA regions appear periodically in a hexagonal pattern^{23–26} such that the boundary channels form a triangular grid as illustrated in Fig. 1(a).

One may expect that the electronic transport in the helical states could be described by a percolation model²⁷ on a triangular network. However, here we show that the helical boundary modes do not form a two-dimensional network, but they are actually independent 1D channels traveling in either of three different directions as shown in Fig. 1(b). The modes propagating in different directions

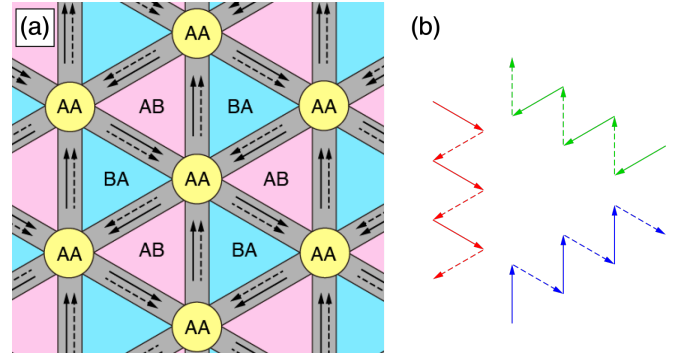


FIG. 1. (a) AB and BA domain structure and helical domain modes in the biased TBG. Here solid and dashed arrows represent independent traveling modes for K valley (mode 1 and 2). (b) Independent 1D eigenmodes in three directions.

are never hybridized at the vertex, and therefore all these states serve as independent perfect 1D channels. The result is consistent with a recent work which predicts the perfect nesting of the Fermi surface in the biased TBG¹⁸.

In the following, we calculate the electronic band structure of the TBG using the continuum-model Hamiltonian and present the band structures for various twist angles and electric field dependencies. The energy band structures show that an applied bias causes two well-defined energy windows which contain sparsely distributed 1D chiral channels, separated by a cluster of nearly flat bands around the charge neutrality point. We also use the tight-binding model to implement arbitrary lattice deformations in TBG, and discuss the effect of lattice relaxation on the 1D channels. Lastly, we explain the origin of these energy windows by a perturbational approach from the small interlayer coupling limit, and also by a two-band model consisting of the intersecting electron and hole bands of single layer graphene. The tunability of the TBG energy dispersion in a perpendicular electric field means there is the potential to explore the param-

eter space where these 1D channels can be found in its experimental realization.

This paper is organized as follows: In Sec. II, we introduce the continuum-model Hamiltonian and describe the formation of 1D states for varying angles and biases. In Sec. III, we consider the effect of lattice relaxation on the 1D channels. Lastly, we explain the origin of these states in Sec. IV, and present a brief conclusion in Sec. V.

II. CONTINUUM MODEL

We calculate the electronic band structure of the twisted bilayer graphene using the continuum model^{1,6-8,28-30}. For a small twist angle, the Hamiltonian is given by

$$H_{\text{TBG}} = \begin{pmatrix} H_1 & U^\dagger \\ U & H_2 \end{pmatrix}, \quad (1)$$

where

$$H_1 = \begin{pmatrix} \frac{\Delta}{2} & -v\pi^\dagger \\ -v\pi & \frac{\Delta}{2} \end{pmatrix}, \quad H_2 = \begin{pmatrix} -\frac{\Delta}{2} & -v\pi^\dagger \\ -v\pi & -\frac{\Delta}{2} \end{pmatrix} \quad (2)$$

and

$$U = u \sum_{j=0,1,2} e^{i\Delta\mathbf{K}_j \cdot \mathbf{r}} \begin{pmatrix} 1 & e^{-i\frac{2\pi}{3}j} \\ e^{i\frac{2\pi}{3}j} & 1 \end{pmatrix}. \quad (3)$$

The Hamiltonian Eq. (1) is equivalent to the continuum-model Hamiltonian derived in^{1,6,28} up to a gauge transformation.^{31,32} The on-diagonal blocks describe the graphene layers 1 and 2 where $\pi = \hbar(\xi k_x + i k_y)$, and the valley index $\xi = \pm 1$ is used to distinguish between K and K' valleys. The parameter v is the band velocity of monolayer graphene where $\hbar v/a = 2.1354$ eV (the lattice constant of graphene is given by $a = 2.46$ Å)^{28,33}, and Δ represents the electrostatic energy shift induced by the perpendicular electric field. The off-diagonal blocks describe the moiré interlayer coupling between the two twisted layers, where the interlayer coupling strength is given by $u = 0.103$ eV. The vectors $\Delta\mathbf{K}_j$ ($j = 0, 1, 2$) account for the shift between the original Brillouin zone corners of the two layers, and are given by

$$\Delta\mathbf{K}_j = \frac{4\pi\theta}{3a} \left[-\sin\left(\frac{2\pi j}{3}\right), \cos\left(\frac{2\pi j}{3}\right) \right], \quad (4)$$

where θ is the twist angle between the two layers in radians.

We calculate the energy spectrum for the K and K' valleys independently as intervalley coupling is negligible at small twist angles. Zone folding is used to bring the states in each valley with momenta connected by the moiré reciprocal lattice vectors, $\mathbf{G}_1 = \Delta\mathbf{K}_1 - \Delta\mathbf{K}_0$ and $\mathbf{G}_2 = \Delta\mathbf{K}_2 - \Delta\mathbf{K}_0$. The basis of k -states of layer 1 and 2 can be taken as

$$\begin{aligned} \mathbf{k}_{m_1, m_2}^{(1)} &= \mathbf{k} + \Delta\mathbf{K}_0 + m_1\mathbf{G}_1 + m_2\mathbf{G}_2 \\ \mathbf{k}_{m_1, m_2}^{(2)} &= \mathbf{k} - \Delta\mathbf{K}_0 + m_1\mathbf{G}_1 + m_2\mathbf{G}_2, \end{aligned} \quad (5)$$

respectively, where \mathbf{k} is the wavenumber in the first moiré Brillouin zone (mBZ) spanned by \mathbf{G}_1 and \mathbf{G}_2 , and m_1 and m_2 are integers. The size of the basis is chosen such that when the Hamiltonian is numerically diagonalized, the energy bands converge up to a cut-off energy.

Figure 2(a) presents the electric field dependence of the TBG band structure for various twist angles, $\theta = 1^\circ, 0.5^\circ, 0.3^\circ$ and 0.2° . The band structures include energy bands from both the K (black) and K' (red) valleys and is shown for the path $\kappa \rightarrow \gamma \rightarrow \mu \rightarrow \kappa'$ in the mBZ illustrated in Fig. 2(b). The original Dirac point of layer 1 is placed at the corner of mBZ at κ' , and the original Dirac point of layer 2 is placed at κ . In increasing Δ , we see that the energy bands are gradually shifted toward zero energy, forming a cluster of nearly flat bands around the charge neutrality point. At the same time, two well-defined energy windows, where energy bands are only sparsely distributed, are formed above and below the zero-energy band cluster. The size of the energy windows are not strongly affected by the size of Δ which can be seen for $\theta = 0.2^\circ$ in increasing Δ .

Most interestingly, is the formation of 1D propagating modes inside the energy windows, which connect the zero-energy band cluster to the bulk bands outside of the energy windows. Figure 2(c) shows a three dimensional plot of the bands from K valley calculated for $\theta = 0.5^\circ$ and $\Delta = 400$ meV, and Fig. 2(d) is the Fermi surface of the same system at $E_F = 50$ meV where black and red lines represent K and K' , respectively. We see that the band dispersion of K is actually composed of three intersecting planes, with band velocities parallel to $(0, -1)$, $(\sqrt{3}/2, 1/2)$ and $(-\sqrt{3}/2, 1/2)$ directions. The different planes are not hybridized with each other, giving nearly straight Fermi lines at the fixed energy. Such straight Fermi surfaces were also reported in the recent paper¹⁸. In the largest bias $\Delta = 400$ meV, we notice some flat levels appear in the upper part of the energy window independently from the dispersive 1D states, (e.g., three horizontal lines in $50 \text{ meV} < |E| < 100 \text{ meV}$ for $\theta = 0.3^\circ$), which can be interpreted as pseudo-Landau levels of the fictitious gauge field¹⁷.

III. EFFECT OF LATTICE RELAXATION

The real TBG is not a simple stack of rigid graphene layers as assumed in the previous section, but it has a spontaneous lattice relaxation and resulting AB/BA domain formation^{23-26,34-42}. Such a structural deformation modifies the electronic band structure^{26,33,40-43}. Here we calculate the energy band structures in the presence of the lattice strain using the tight-binding method²⁶. The Hamiltonian is given by

$$H = - \sum_{i,j} t(\mathbf{R}_i - \mathbf{R}_j) |\mathbf{R}_i\rangle \langle \mathbf{R}_j| + \text{h.c.} \quad (6)$$

where \mathbf{R}_i is the atomic coordinate, $|\mathbf{R}_i\rangle$ is the wave function at site i , and $t(\mathbf{R}_i - \mathbf{R}_j)$ is the transfer integral be-

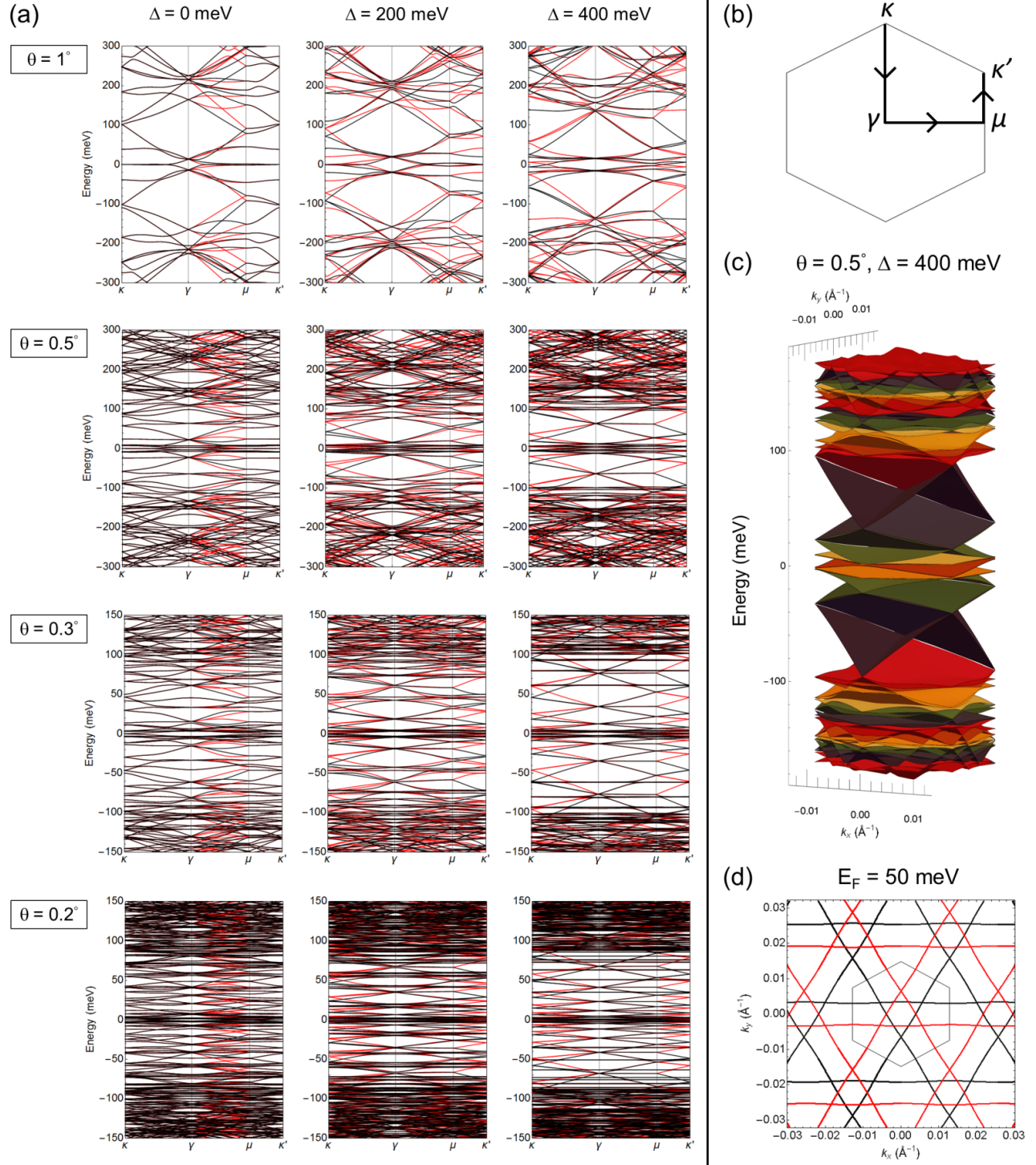


FIG. 2. (a) Band structure of the twisted bilayer at various twist angles and varying Δ , calculated using the continuum model. (b) The moiré Brillouin zone. (c) A three dimensional plot of K -valley bands, and (d) the contour plot at $E_F = 50$ meV, calculated for $\theta = 0.5^\circ$ and $\Delta = 400$ meV. The black and red lines represent K and K' valleys, respectively.

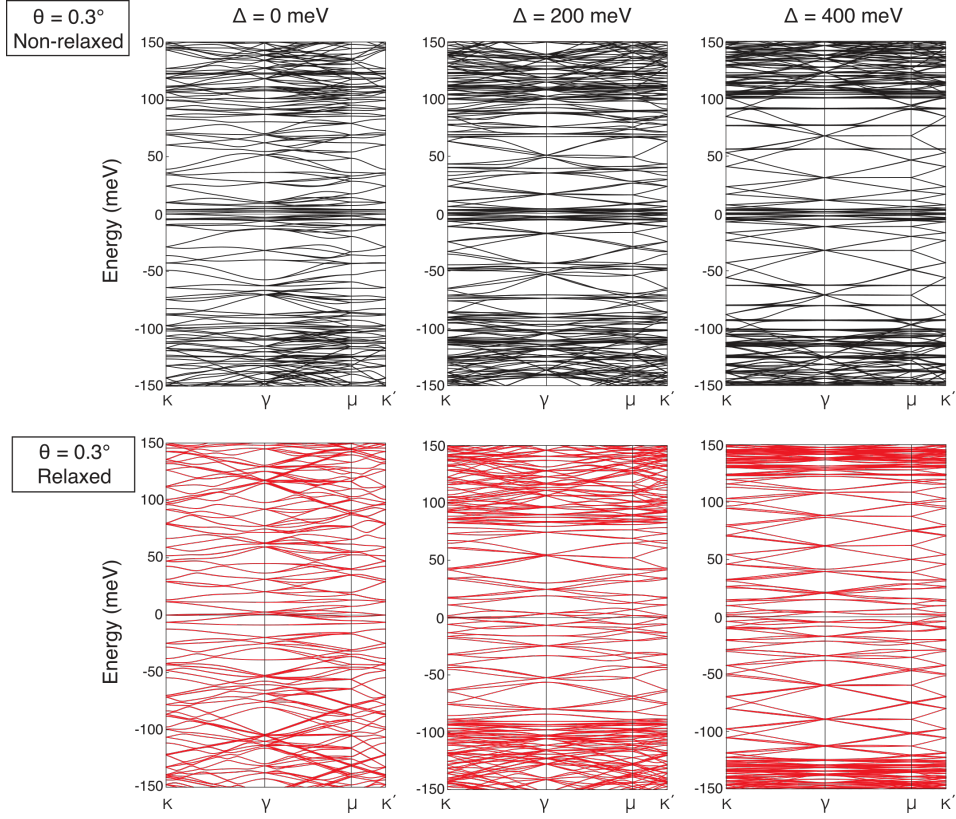


FIG. 3. Band structure of non-relaxed (upper panels) and relaxed (lower panels) TBGs in $\theta = 0.3^\circ$ and different Δ 's and calculated using the tight-binding model.

tween atom i and j . We adopt the Slater-Koster type formula for the transfer integral⁴⁴,

$$-t(\mathbf{d}) = V_{pp\pi}(d) \left[1 - \left(\frac{\mathbf{d} \cdot \mathbf{e}_z}{d} \right)^2 \right] + V_{pp\sigma}(d) \left(\frac{\mathbf{d} \cdot \mathbf{e}_z}{d} \right)^2, \quad (7)$$

$$V_{pp\pi}(d) = V_{pp\pi}^0 \exp \left(-\frac{d - a_0}{r_0} \right), \quad (8)$$

$$V_{pp\sigma}(d) = V_{pp\sigma}^0 \exp \left(-\frac{d - d_0}{r_0} \right), \quad (9)$$

where $\mathbf{d} = \mathbf{R}_i - \mathbf{R}_j$ is the distance between two atoms and \mathbf{e}_z is the unit vector on z axis. $V_{pp\pi}^0 \approx -2.7$ eV is the transfer integral between nearest-neighbor atoms of monolayer graphene which are located at distance $a_0 = a/\sqrt{3} \approx 0.142$ nm, $V_{pp\sigma}^0 \approx 0.48$ eV is the transfer integral between two nearest-vertically aligned atoms and $d_0 \approx 0.334$ nm is the interlayer spacing. The decay length r_0 of transfer integral is chosen as $0.184a$ so that the next nearest intralayer coupling becomes $0.1V_{pp\pi}^0$. At $d > \sqrt{3}a$, the transfer integral is very small and negligible. The optimized atomic positions are obtained by the method introduced in the previous work²⁶. Using this, we construct the tight-binding Hamiltonian of the relaxed TBG and calculate the energy bands.

Figure 3 compares the electronic band structure of non-relaxed (upper panels) and relaxed (lower panels) TBGs in $\theta = 0.3^\circ$ and different Δ 's. In the tight-binding model, the valleys are not distinguished. We see that the energy bands of the non-relaxed calculation quantitatively agree with those in the continuum method in Fig. 2. In the presence of the relaxation, we confirm that the qualitative feature remains the same: we still see the energy windows and the 1D chiral states. The major difference from the non-relaxed state is that the central pseudo-Landau levels mentioned in the previous section are completely hybridized with 1D chiral states, and become a part of the dispersive bands. Also we notice that the bands in the zero-energy cluster become less flat and a bit more dispersive.

Figure 4 shows typical wave functions in the energy window in the non-relaxed TBG and the relaxed TBG of $\theta = 0.55^\circ$ and $\Delta = 400$ meV. Here we chose the corresponding states in non-relaxed and relaxed cases, which are connected by a continuous increase of the relaxation. The state is chosen from a 1D band of the electron side with the velocity along k_y axis ($\kappa - \gamma$ direction in this figure). In each case, we observe that the wave function takes a 1D form extending along y direction, while it is disconnected in the perpendicular direction. The states in the different Fermi surface branches at the same energy are obtained by $\pm 120^\circ$ rotation of this figure. We

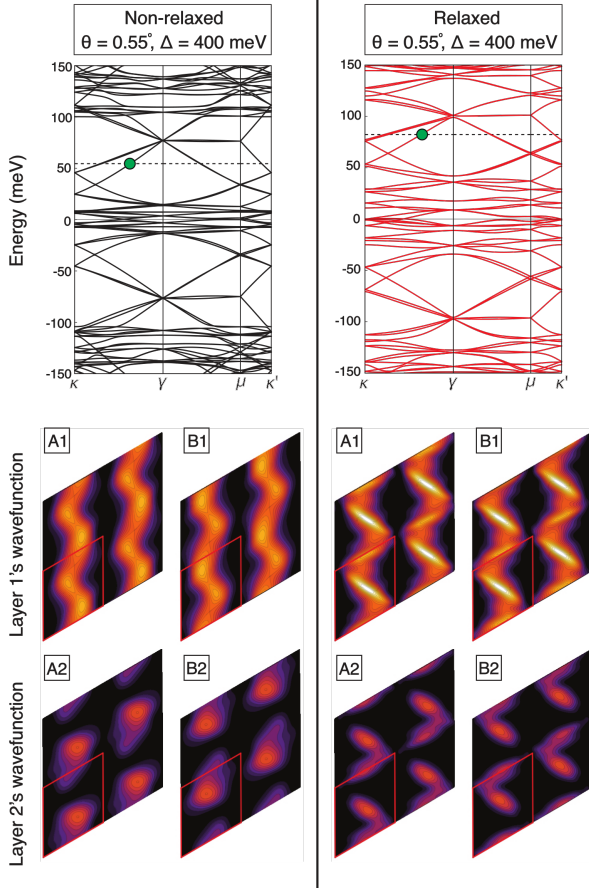


FIG. 4. Energy spectrum and the wave function of a typical state at K valley in the energy window (indicated in the spectrum) calculated for the non-relaxed TBG and the relaxed TBG of $\theta = 0.55^\circ$ and $\Delta = 400$ meV. The plot of the wave function represents squared amplitude on sublattice A_1 , B_1 , A_2 and B_2 separately, where a red rhombus indicates a single moiré unit cell.

confirm that the local current density is along $-y$ direction, in accordance with the negative band velocity in the k_y direction. The wave amplitude is mainly concentrated on the layer 1, while it is concentrated on layer 2 in the hole side states.

In the presence of the lattice relaxation, we see that the wave function becomes more localized on the AB-BA boundary. This is natural because the AB and BA regions (where the energy band is gapped out) significantly expand under the lattice relaxation²⁶, and the wave amplitude must be confined to the narrow boundary region. The similar, zigzag-shaped wave function was also reported in a recent work¹⁸. Interestingly, we see that the relaxed TBG's wave function in Fig. 4 has its amplitude not on the boundary along y , but only on the boundary in the two other directions along $(\sqrt{3}/2, -1/2)$ and $(-\sqrt{3}/2, -1/2)$. With closer inspection, we also find that it has different structures between the boundaries along $(\sqrt{3}/2, -1/2)$ and $(-\sqrt{3}/2, -1/2)$, although the atomic structures are completely symmetric. Recalling that each

single boundary has two different traveling modes (denoted as mode 1 and 2) as mentioned, this result suggests that, at every vertex of the triangular grid (AA region), mode 1 is always scattered to mode 2 in -120° direction, while mode 2 is always scattered to mode 1 in $+120^\circ$ direction. As a result, we have three independent, zigzag traveling modes as illustrated in Fig. 1(b).

IV. ORIGIN OF THE 1D CHIRAL CHANNELS

The origin of the energy window and the 1D channels can be intuitively understood by a perturbational approach from the small interlayer coupling limit. Figure 5 shows the band structure of the continuum model in Eq. (1), with $\theta = 0.3^\circ$ and $\Delta = 400$ meV, and with increasing interlayer coupling u from zero to the actual value in TBG. With small u , we see that two gaps open in the electron side and the hole side, and they eventually become the window regions in the full u parameter. We see that the 1D channel states always remain inside the gap, preventing the spectrum from becoming fully gapped. The width of the energy window is obviously the order of u . The energy bands between the two gaps are squashed with increasing u , and finally becomes the zero-energy band cluster.

The opening of the two gaps in small u can be explained by considering the following two-band model. In a large Δ , the low energy region is dominated by the hole band of graphene layer 1 and the electron band of layer 2. While considering the interlayer coupling U , we can imagine that the two opposite conical bands of single layer graphenes are crossing with each other with a relative momentum shift of $\Delta\mathbf{K}_j$ ($j = 0, 1, 2$), and the band anti-crossing occurs at the cross section. Figure 6(a) illustrates the actual crossing lines between the Dirac cones in the case of $\theta = 0.3^\circ$ and $\Delta = 200$ meV, where three circles (red, blue and green) correspond to $j = 0, 1, 2$.

The size of the gap is roughly proportional to the matrix element of U between the two states on the crossing line. The graphene's eigenstates are written in the (A, B) spinor representation as

$$|\mathbf{k}, s\rangle = \frac{1}{\sqrt{2}} \begin{pmatrix} 1 \\ -se^{i\theta(\mathbf{k})} \end{pmatrix}, \quad (10)$$

where $s = \pm$ represent the conduction and valence bands, respectively, and $\theta(\mathbf{k}) = \arctan(k_y/k_x)$. Now, the matrix element of U from graphene 1 to graphene 2 is

$$\langle \mathbf{k} + \Delta\mathbf{K}_j, + | U | \mathbf{k}, - \rangle \approx iu \sin \left[\theta(\mathbf{k}) - \frac{2\pi j}{3} \right], \quad (11)$$

where $|\Delta\mathbf{K}_j| \ll |\mathbf{k}|$ is assumed. In Fig. 6(b), the thickness of the crossing lines represents the amplitude of the interlayer matrix element on the Dirac cones of layer 1 and 2, respectively. We see the matrix element vanishes near $E = 0$, and this is the reason why the two major gaps open above and below $E = 0$.

The 1D channels remaining inside the energy window can be explained by the reconstruction of the Fermi surface. Figures 6(c) and (d) illustrate the Fermi surfaces before introducing u at $E_F = 20$ meV, which is slightly below the maximum energy of the crossing rings. In panel (c), the central dashed circle represents the hole band of layer 1, and the three solid circles are the electron band of layer 2 with three momentum shifts $\Delta\mathbf{K}_j$ ($j = 0, 1, 2$). In panel (d), the Fermi surface of layer 1 is centered instead. The hybridized Fermi surfaces after the infinitesimal anti-crossing are shown in Fig. 6(e). We therefore have three open Fermi surfaces that are 120 degrees apart as well as three closed pockets. By increasing u , the closed pockets are gapped out due to a good nesting between the electron and hole parts. On the other hand, the open Fermi surfaces remain ungapped, which explains the origin of the 1D chiral channels filling the gap. We also see that the open Fermi surface mainly consists of the layer 1 component (solid line) which is consistent with the fact that the wave function has larger amplitude on layer 1 in Fig. 4.

In this picture, we only consider the band crossing of the first order in u , while we actually have high-order hybridization at other crossing points. It is somewhat surprising that the 1D chiral states in three directions are not hybridized and remain independent even in a large u beyond the perturbational regime. This is understood by the k -space map of the interlayer matrix element in Fig. 7, where open circles represent the graphene 1's hole states at $\mathbf{k}_{m_1, m_2}^{(1)}$, filled circles the graphene 2's electron states at $\mathbf{k}_{m_1, m_2}^{(2)}$, and the bond thickness is proportional to the matrix element of U between the two states. We can show that the 1D chiral states in the positive energy window are contributed by graphene's states only in the regions I, III and V, and those in the negative energy window are by the regions II, IV and VI. This is consistent with the observation that the open Fermi surface in Fig. 6(e) consists of the graphene's Fermi surface portions in the same regions. We see that the matrix element nearly vanishes on the boundary of different regions (dashed lines) according to Eq. (11), except for the k -points near the origin which do not contribute to the low-energy states. As a result, the six regions I, II, \dots VI are nearly decoupled and that is why the 1D channels running in the different directions remain independent in increasing u .

The perfect 1D channels in the biased TBG is analogous to those in zigzag graphene nanoribbons⁴⁵. In a doped zigzag nanoribbon, it is known that each valley has different numbers of left-moving modes and right-moving modes at the Fermi energy; n right modes and $n + 1$ left modes at one valley, while $n + 1$ right modes and n left modes at the other valley. The excess traveling mode in each valley remains as a perfectly conducting channel even in the disordered system, as long as the impurities are long-ranged and do not mix the different valleys. The perfect 1D channels in biased TBG can be viewed as a 2D

version of this, in that each single sector of I, III and V has different numbers of out-going modes and in-coming modes (with respect to the graphene's Fermi circle), as is clear from different arc lengths of the electron and hole Fermi surfaces in Fig. 6(e), and that different sectors are not hybridized by the interlayer coupling u . Therefore the excess modes originate from the electron Fermi surface and they remain as traveling modes in the presence of u .

The disorder effect on these 1D channels is an important problem when considering the electronic transport. As shown in Fig. 1(b), each 1D channel is composed of straight parts on the AB-BA boundary and corner angles on AA spots. A hybridization of different 1D channels takes place only by a local mixing of the mode 1 and 2 on the AB-BA boundaries, or an irregular reflection at the AA corners. In real TBGs, the moiré structure exhibits a distorted triangular pattern with shifted AA spots and extended / shortened AB-BA boundaries²³⁻²⁵. However, we expect that such a moiré-scale distortion would not cause a strong mixing of different 1D channels, because the local atomic structures of AA and AB-BA boundary are not modified very much⁴⁶, such that the hubs and the links in the triangular lattice work in the same way as in the non-distorted system. Major scatterings should be mainly caused by short-ranged disorder smaller than the local structures of AB-BA boundary and AA spots (which is about a few nm). The detailed study on the disorder scattering will be left for future works.

V. CONCLUSION

We used the continuum-model and tight-binding Hamiltonians to show that TBGs with an applied bias exhibit perfect 1D channels in well-defined energy windows on either side of zero energy. We found that these states never hybridise and they propagate independently in three different directions along the domain walls separating AB and BA regions. In the presence of arbitrary lattice deformations, we show that the wave functions become even more localized on the domain boundaries. The formation of the well-defined energy windows and the origin of these states is explained by the two-band model consisting of the intersecting electron and hole bands of single layer graphene, where the 1D channels correspond to the emergent open Fermi surfaces formed by the moiré interlayer hybridization.

VI. ACKNOWLEDGMENTS

BT acknowledges financial support from the Japan Society for the Promotion of Science as a JSPS International Research Fellow (Summer Programme 2019), EP-SRC Doctoral Training Centre Graphene NOWNANO EP/L01548X/1 and the Lloyd's Register Foundation Nanotechnology grant. MK acknowledges the financial support of JSPS KAKENHI Grant Number JP17K05496.

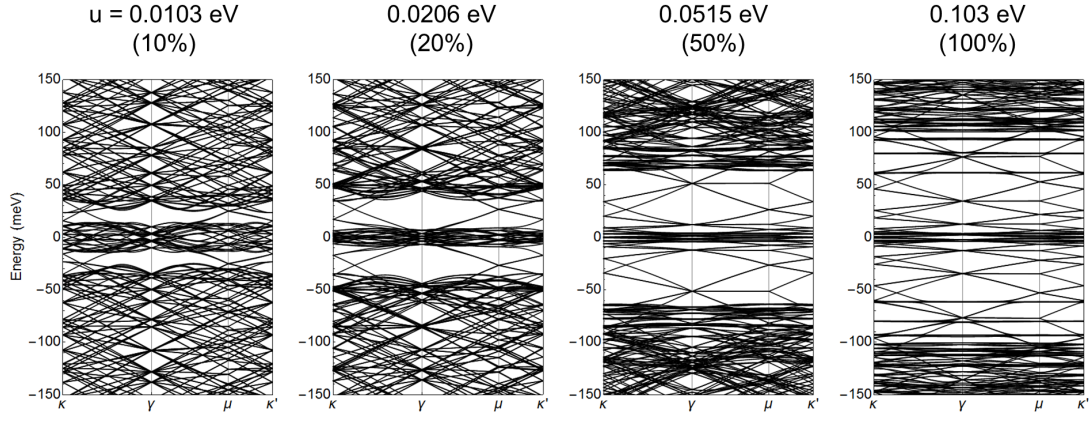


FIG. 5. Band structure of the continuum model for the TBG with $\theta = 0.3^\circ$ and $\Delta = 400$ meV, and the interlayer coupling u from zero to the actual value in TBG.

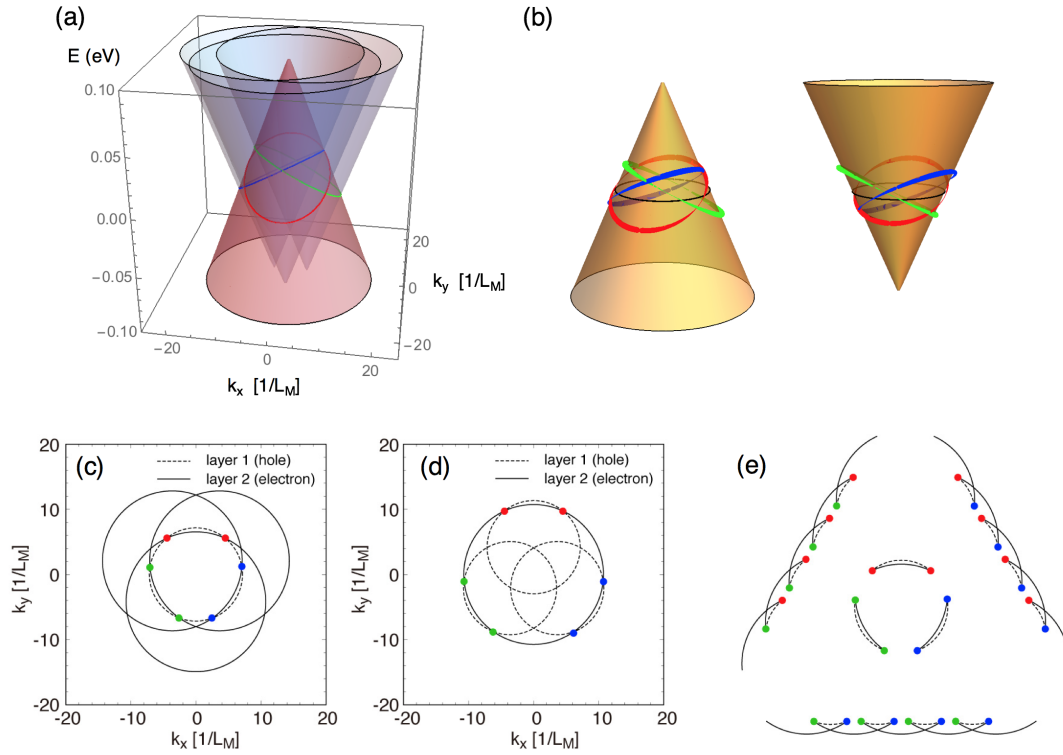


FIG. 6. (a) Crossing lines between the Dirac cones, where three circles (red, blue and green) correspond to $j = 0, 1, 2$. Here we take $\theta = 0.3^\circ$ and $\Delta = 200$ meV. (b) Amplitude of the interlayer matrix element on the crossing lines on the Dirac cones of layer 1 and 2. (c), (d) Relative positions of the Fermi surfaces of layer 1 (dashed) and layer 2 (solid), in absence of u and at $E_F = 20$ meV. (e) Schematic diagram showing the Fermi surfaces and the crossing lines in the k_x - k_y plane.

¹ J. M. B. Lopes dos Santos, N. M. R. Peres, and A. H. Castro Neto, “Graphene bilayer with a twist: Electronic structure,” *Phys. Rev. Lett.* **99**, 256802 (2007).

² E. J. Mele, “Commensuration and interlayer coherence in twisted bilayer graphene,” *Phys. Rev. B* **81**, 161405 (2010).

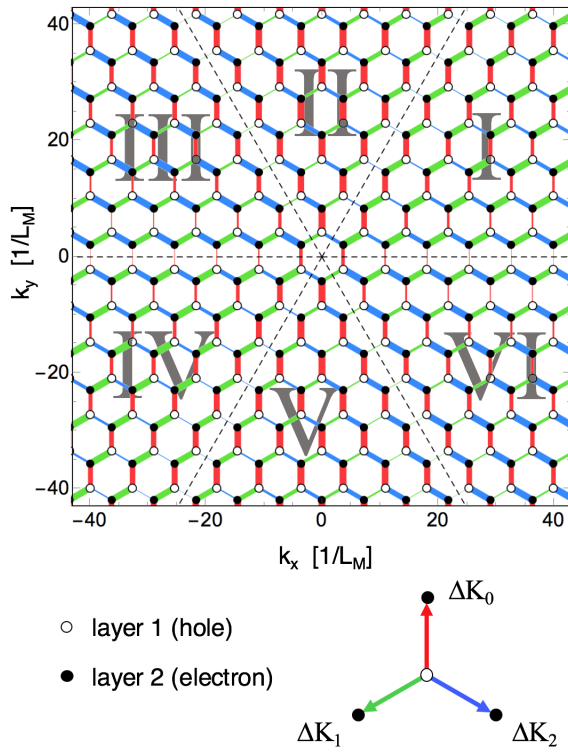


FIG. 7. Map of the interlayer matrix element, where open circles represent the hole states at $\mathbf{k}_{m_1, m_2}^{(1)}$ of single-layer graphene 1, and filled circles the electron states at $\mathbf{k}_{m_1, m_2}^{(2)}$ of graphene 2, where $\mathbf{k} = 0$ is chosen in Eq. (5). The bond thickness is proportional to the matrix element of U between the two states.

- ³ G. Trambly de Laissardière, D. Mayou, and L. Magaud, “Localization of dirac electrons in rotated graphene bilayers,” *Nano Lett.* **10**, 804–808 (2010).
- ⁴ S. Shallcross, S. Sharma, E. Kandelaki, and O. A. Pankratov, “Electronic structure of turbostratic graphene,” *Phys. Rev. B* **81**, 165105 (2010).
- ⁵ E. S. Morell, J. D. Correa, P. Vargas, M. Pacheco, and Z. Barticevic, “Flat bands in slightly twisted bilayer graphene: Tight-binding calculations,” *Phys. Rev. B* **82**, 121407 (2010).
- ⁶ R. Bistritzer and A. H. MacDonald, “Moiré bands in twisted double-layer graphene,” *Proc. Natl. Acad. Sci.* **108**, 12233 (2011).
- ⁷ M. Kindermann and P. N. First, “Local sublattice-symmetry breaking in rotationally faulted multilayer graphene,” *Phys. Rev. B* **83**, 045425 (2011).
- ⁸ J. M. B. Lopes dos Santos, N. M. R. Peres, and A. H. Castro Neto, “Continuum model of the twisted graphene bilayer,” *Phys. Rev. B* **86**, 155449 (2012).
- ⁹ P. Moon and M. Koshino, “Energy spectrum and quantum hall effect in twisted bilayer graphene,” *Phys. Rev. B* **85**, 195458 (2012).
- ¹⁰ G. Trambly de Laissardière, D. Mayou, and L. Magaud, “Numerical studies of confined states in rotated bilayers of graphene,” *Phys. Rev. B* **86**, 125413 (2012).
- ¹¹ Y. Cao, V. Fatemi, K. Fang, S. and Watanabe, T. Taniguchi, E. Kaxiras, and P. Jarillo-Herrero, “Uncon-

- ventional superconductivity in magic-angle graphene superlattices,” *Nature* **556**, 43 (2018).
- ¹² Y. Cao, V. Fatemi, A. Demir, S. Fang, S. L. Tomarken, J. Y. Luo, J. D. Sanchez-Yamagishi, K. Watanabe, T. Taniguchi, E. Kaxiras, R. C. Ashoori, and P. Jarillo-Herrero, “Correlated insulator behaviour at half-filling in magic-angle graphene superlattices,” *Nature* **556**, 80 (2018).
- ¹³ M. Yankowitz, S. Chen, H. Polshyn, Y. Zhang, K. Watanabe, T. Taniguchi, D. Graf, A. Young, and C. R. Dean, “Tuning superconductivity in twisted bilayer graphene,” *Science* **363**, 1059–1064 (2019).
- ¹⁴ L. Xian, S. Barraza-Lopez, and M. Y. Chou, “Effects of electrostatic fields and charge doping on the linear bands in twisted graphene bilayers,” *Phys. Rev. B* **84**, 075425 (2011).
- ¹⁵ P. San-Jose and E. Prada, “Helical networks in twisted bilayer graphene under interlayer bias,” *Phys. Rev. B* **88**, 121408 (2013).
- ¹⁶ P. Moon, Y.-W. Son, and M. Koshino, “Optical absorption of twisted bilayer graphene with interlayer potential asymmetry,” *Physical Review B* **90**, 155427 (2014).
- ¹⁷ A. Ramires and J. L. Lado, “Electrically tunable gauge fields in tiny-angle twisted bilayer graphene,” *Phys. Rev. Lett.* **121**, 146801 (2018).
- ¹⁸ M. Fleischmann, R. Gupta, F. Wulfschläger, D. Weckbecker, V. Meded, S. Sharma, B. Meyer, and S. Shallcross, “Perfect and controllable nesting in the small angle twist bilayer graphene,” *arXiv preprint arXiv:1908.08318* (2019).
- ¹⁹ E. McCann, “Asymmetry gap in the electronic band structure of bilayer graphene,” *Phys. Rev. B* **74**, 161403 (2006).
- ²⁰ A. Vaezi, Y. Liang, D. H. Ngai, L. Yang, and E.-A. Kim, “Topological edge states at a tilt boundary in gated multilayer graphene,” *Phys. Rev. X* **3**, 021018 (2013).
- ²¹ F. Zhang, A. H. MacDonald, and E. J. Mele, “Valley chern numbers and boundary modes in gapped bilayer graphene,” *PNAS* **110**, 10546–10551 (2013).
- ²² M. Koshino, “Electron delocalization in bilayer graphene induced by an electric field,” *Phys. Rev. B* **78**, 155411 (2008).
- ²³ L. Brown, R. Hovden, P. Huang, M. Wojcik, D. A. Muller, and J. Park, “Twinning and twisting of tri- and bilayer graphene,” *Nano Lett.* **12**, 1609–1615 (2012).
- ²⁴ J. Lin, W. Fang, W. Zhou, A. R. Lupini, J. C. Idrobo, J. Kong, S. J. Pennycook, and S. T. Pantelides, “AC/AB stacking boundaries in bilayer graphene,” *Nano Lett.* **13**, 3262–3268 (2013).
- ²⁵ J. S. Alden, A. W. Tsen, P. Y. Huang, R. Hovden, L. Brown, J. Park, D. A. Muller, and P. L. McEuen, “Strain solitons and topological defects in bilayer graphene,” *Proc. Natl. Acad. Sci. USA* **110**, 11256–11260 (2013).
- ²⁶ N. N. T. Nam and M. Koshino, “Lattice relaxation and energy band modulation in twisted bilayer graphene,” *Phys. Rev. B* **96**, 075311 (2017).
- ²⁷ J. T. Chalker and P. D. Coddington, “Percolation, quantum tunnelling and the integer hall effect,” *Journal of Physics C: Solid State Physics* **21**, 2665 (1988).
- ²⁸ P. Moon and M. Koshino, “Optical absorption in twisted bilayer graphene,” *Phys. Rev. B* **87**, 205404 (2013).
- ²⁹ M. Koshino, “Interlayer interaction in general incommensurate atomic layers,” *New J. Phys.* **17**, 015014 (2015).

- ³⁰ M. Koshino and P. Moon, “Electronic properties of incommensurate atomic layers,” *J. Phys. Soc. Jpn.* **84**, 121001 (2015).
- ³¹ G. Tarnopolsky, A. J. Kruchkov, and A. Vishwanath, “Origin of magic angles in twisted bilayer graphene,” *Phys. Rev. Lett.* **122**, 106405 (2019).
- ³² J. Liu, J. Liu, and X. Dai, “Pseudo landau level representation of twisted bilayer graphene: Band topology and implications on the correlated insulating phase,” *Phys. Rev. B* **99**, 155415 (2019).
- ³³ M. Koshino, N. F. Q. Yuan, T. Koretsune, M. Ochi, K. Kuroki, and L. Fu, “Maximally localized wannier orbitals and the extended hubbard model for twisted bilayer graphene,” *Phys. Rev. X* **8**, 031087 (2018).
- ³⁴ A. M. Popov, I. V. Lebedeva, A. A. Knizhnik, Y. E. Lozovik, and B. V. Potapkin, “Commensurate-incommensurate phase transition in bilayer graphene,” *Phys. Rev. B* **84**, 045404 (2011).
- ³⁵ K. Uchida, S. Furuya, J.-I. Iwata, and A. Oshiyama, “Atomic corrugation and electron localization due to moiré patterns in twisted bilayer graphenes,” *Phys. Rev. B* **90**, 155451 (2014).
- ³⁶ M. M. van Wijk, A. Schuring, M. I. Katsnelson, and A. Fasolino, “Relaxation of moiré patterns for slightly misaligned identical lattices: graphene on graphite,” *2D Mater.* **2**, 034010 (2015).
- ³⁷ S. Dai, Y. Xiang, and D. J. Srolovitz, “Twisted bilayer graphene: Moiré with a twist,” *Nano Lett.* **16**, 5923–5927 (2016).
- ³⁸ S. K. Jain, V. Juričić, and G. T. Barkema, “Structure of twisted and buckled bilayer graphene,” *2D Mater.* **4**, 015018 (2016).
- ³⁹ S. Carr, D. Massatt, S. B. Torrisi, P. Cazeaux, M. Lusk, and E. Kaxiras, “Relaxation and domain formation in incommensurate two-dimensional heterostructures,” *Phys. Rev. B* **98**, 224102 (2018).
- ⁴⁰ X. Lin, D. Liu, and D. Tománek, “Shear instability in twisted bilayer graphene,” *Phys. Rev. B* **98**, 195432 (2018).
- ⁴¹ H. Yoo, R. Engelke, S. Carr, S. Fang, K. Zhang, P. Cazeaux, S. H. Sung, R. Hovden, A. W. Tsen, T. Taniguchi, K. Watanabe, G.-C. Yi, M. Kim, M. Lusk, E. B. Tadmor, E. Kaxiras, and P. Kim, “Atomic and electronic reconstruction at the van der waals interface in twisted bilayer graphene,” *Nat. Mater.* **18**, 448 (2019).
- ⁴² F. Guinea and N. R. Walet, “Continuum models for twisted bilayer graphene: Effect of lattice deformation and hopping parameters,” *Phys. Rev. B* **99**, 205134 (2019).
- ⁴³ P. Lucignano, D. Alfè, V. Cataudella, D. Ninno, and G. Cantele, “Crucial role of atomic corrugation on the flat bands and energy gaps of twisted bilayer graphene at the magic angle $\theta \sim 1.08^\circ$,” *Phys. Rev. B* **99**, 195419 (2019).
- ⁴⁴ J. C. Slater and G. F. Koster, “Simplified lcao method for the periodic potential problem,” *Phys. Rev.* **94**, 1498 (1954).
- ⁴⁵ K. Wakabayashi, Y. Takane, and M. Sigrist, “Perfectly conducting channel and universality crossover in disordered graphene nanoribbons,” *Physical review letters* **99**, 036601 (2007).
- ⁴⁶ M. Koshino and Y.-W. Son, “Moiré phonons in twisted bilayer graphene,” *Phys. Rev. B* **100**, 075416 (2019).